Investigation of particle and molecular extinction effects in remote sensing by ultraviolet DIAL in the lower atmosphere

Gholamreza Shayeganrad[*1] and Leila Mashhadi[2], Davood Momeni[1]
[1]Physics Department, Islamic Azad University, Karaj Branch, Karaj, Iran,
member of OSA, Email: shayeganrad@yahoo.com
[2]Physics Department, Amirkabir University of Technology, Tehran, Iran,
member of OSA

Abstract

This study presents theoretical investigation of the effects of particle and molecular extinction in horizontal remote sensing near the ground for several visibilities at UV wavelengths by neglecting the spatial inhomogeneity of aerosol in the atmosphere and taking into account the dependence of refracting on air temperature and pressure. Due to weak attenuation of oxygen and other gaseous atmospheric constituents in this region, we have only considered the effect of ozone in calculation. The results are important to estimate systematic errors in measuring gas concentration introduced by large wavelength separation in UV-DIAL. The total attenuation (km^{-1}) at wavelengths is listed in the form of a table from 200 to 400 nm for several values of visibilities. It is found the aerosol attenuation in UV region varies quite smoothly with wavelength and therefore systematic error caused by aerosol scattering is negligible in remote sensing by UV-DIAL even with large wavelength separation.

Moreover, it has been found that only aerosol extinction is dominant in lidar remote sensing in the lower atmosphere in UV region. In large altitude that aerosol concentration is lower; the molecular scattering is important especially for wavelengths larger than 310 nm.

Key words: Lidar, differential absorption lidar, remote sensing, ultraviolet wavelength, troposphere, systematic error, differential aerosol extinction, differential molecular scattering, differential absorption by ozone

* **Corresponding author**
Gholamreza Shayeganrad
E-mail: shayeganrad@yahoo.com
Physics Department, Islamic Azad University, Karaj Branch, Karaj, Iran

1. Introduction

Optical detection and monitoring methods are well known to provide remote sensing with the unique advantages such as high selectivity, high sensitivity, wide dynamic range, fast response, good temporal resolution, noninvasiveness and nondestructiveness and possibility of non-contact hazardous plume measurement. Since the initial development of laser, a large number of liner and nonlinear laser-based analysis techniques for gas-phase remote sensing in different environments have been developed. The most common principle employed for the detection of environmental pollutants involves the interaction of the trace species with laser light (absorption and scattering) (Sigrist, 1994; Meyers, 2000; Mandelis and Hess, 1997; Demtröder, 2003; Weitkamp, 2005; Holton et al., 2002; Camagani and Sandroni, 1984; Hering et al., 2003; Thomas, 1995; Fujii and Fukuahi, 2005; Dell'Aglioet al., 2002).

Among these techniques, the lidar technique has been proved to be a very reliable instrument for high temporal and spatial monitoring and measuring atmospheric properties like aerosol, neutral density, temperature and concentration of various species in the troposphere with high horizontal and vertical resolution and the high range of measurements from a few meters to several kilometers. In addition, differential absorption lidar (DIAL) includes high sensitivity, good spatial resolution for long-range dynamic monitoring and the capability of wavelength scanning over a wide variety of molecules and atoms having absorption characteristic in the spectral range as well as the quantitative evaluation of desired species (Thomas, 1995; Fujii and Fukuahi, 2005; Zanzottera, 1990; Uchino, 2006; Wolf et al., 1993; Kobayashi et al., 2004; Edner et al. 1987; Beniston et al., 1990). In the ultraviolet spectral range, a large number of trace species, such as ozone (Derava et al. 2004; Veselovskii and Barchunov, 1999; Moosmüller et al., 1992; Moosmüller et al., 1994; Browell et al., 1991; Fugii et al., 2001; Egeback, 1984; Rothe et al., 1992), sulfur dioxide (Milton et al., 1992; Edner et al., 1989), nitric oxide (Derava et al., 2004), nitric dioxide (Moosmüller et al., 1994), benzene (Rothe et al., 1992), toluene (Milton et al., 1992) and mercury (Edner et al., 1989) have been measured successfully by using the DIAL technique.

Description of lidar technique is provided in earlier papers and is summarizes here. It consists of a transmitter and a receiver. The transmitter emits short-time laser pulses (typically 10-20 ns in duration) into the atmosphere. The laser beam interacts with the atmospheric constituents as it propagates; through a multitude of phenomena such as elastic light scattering (molecular-Rayleigh, aerosols-Mie), and inelastic (molecular–Raman) light scattering, fluorescence and absorption. Scattering is dependent to some parameters such as wavelength, molecular density and size of the scatter as well as distance between the transmitter and receiver; larger density and distance scattering is more. Usually, scattering leads to a decrease of the transmitted energy similar to absorption. It is reason to arrive photons to a detector which is not placed in the propagation direction. In the atmosphere, oxygen, nitrogen, ozone, aerosols have the greatest contribution in the scattering. Rayleigh scattering is observed from particles with dimension smaller than the wavelength of the light without absorbing the light and Mie scattering take place at particles of size of order of light wavelength (~0.1-10 μm).

Scattering and absorption are two basic mechanisms for the detection of signal. A receiving telescope collects a very small fraction of the backscattered light. The receiver usually contains a polychromatic filter for the spectral separation and reduces the background noise, high sensitivity photodetectors, and fast sampling rate analog-to-digital converters. The magnitude of the received signal is proportional to the number density of the atmospheric scatters (molecules or aerosols), their intrinsic properties (cross–section) and the laser incident energy.

On the other hand, the DIAL technique is based on the spectral absorption of the species and elastic scattering (Rayleigh and Mie) and requires at least two different closely spaced wavelengths which send subsequently to the atmosphere. Those are close to each other with a large absorption coefficient difference, one at the tuned line, λ_{on}, where the species under investigation absorb and the other at a non-absorbing detuned line, λ_{off}. The first line is attenuated by absorption and the second one measures the density of aerosols and molecules as in standard lidar systems. The difference in intensity of the two return signals can be used

to deduce the concentration of investigated species, aerosol number density and sizes, while the time delay indicates the distance between the lidar and scattered particles.

In the field of remote sensing the propagation of light and attenuation characteristics of the atmosphere and target are obviously important. The main error source is high aerosol and trace gas concentrations in the troposphere, so the choice of DIAL wavelengths becomes very critical. Before a DIAL system is designed, the differential extinction of the atmosphere must be known to derive the necessary parameters such as wavelength selection, determine of laser energy and pulse duration based on detector parameters, background light level and maximum range detection. Moreover, sunphotomete sensors systems design require knowledge of the attenuation of the atmosphere on the received signal.

The accuracy, sensitivity and lower detection limit of the DIAL measurement is directly dependent on the accuracy of the differential extinction of the atmosphere and differential absorption cross section species of interest. Both of them lead to additional error, first called systematic error and the second named as statistical error.

The attenuation of the light by the atmosphere is one of the major problems in remote sensing and measurement of optical radiation. The problem is evident in absolute measurement by LIF, LIBS and Raman lidar, that inelastic backscatter signal is affected by aerosol extinction, and neglecting the atmospheric attenuation leads to an uncertainty in measurement. Also, for certain applications where absorption mechanism is important, laser wavelength is chosen such that it does not have absorption band of any molecule/specie at that wavelength.

Moreover, this problem is typically appeared in DIAL measuring concentration when the wavelength is sufficiently separated. Most analysis of DIAL measurement ignore the errors due to difference in atmospheric backscattering, aerosol extinction, and Rayleigh scattering at on and off wavelengths. Errors can arise in this approach when the wavelengths are significantly separated and there is range dependence in the aerosol scattering distribution. Moreover, because of the dependence of attenuation to distance, knowing the value of atmospheric attenuation is useful to relative measurements of radiant sources which are located at different distance of photodetector.

The aim of this study is to establish of the effects of attenuation of aerosols and atmospheric constituents in propagation of ultraviolet light in the tower atmosphere to correct uncertainty in measurements in remote sensing by lidar and DIAL. In different wavelength work accurate measurements of the attenuation as a function of wavelength are required.

We have provided a table for total attenuation for horizontal propagation of light in lower atmosphere at UV wavelength from 200 to 400 nm. Moreover, it is useful to establish the systematic errors in remote sensing of pollutants in the environment by DIAL.

2. Systematic errors

The back-scattered power observed at the detector from distance R is given by the Lidar equation:

$$P_s(\lambda, R) = K \frac{\beta(\lambda, R))}{R^2} e^{-2\tau(\lambda,R)} \quad (1)$$

where P_s is instantaneous power received by the detector from the range R, $\beta(\lambda,R)$ is the back-scattering coefficient and the optical depth $\tau(\lambda, R) = \int_0^R \alpha(\lambda, r)dr$ is the integral of the extinction coefficient $\alpha(\lambda,R)$ along the path. The constant K combines all device dependent parameters and is particular proportional to the telescope area and the geometrical compression.

Usually backscatter coefficient β for elastically backscattered light consist of contribution from both air molecules and aerosols, i.e. $\beta(\lambda, R) = \beta_{ms} + \beta_{as}$. The molecular backscatter and extinction coefficient differs by a constant factor $\beta_{ms} = 3/(8\pi)\alpha_{ms}$ and can easily be substituted, while for the aerosol coefficients, this procedure is not possible and must define "lidar-ratio" as:

$$S(\lambda, R) = \frac{\alpha_{as}}{\beta_{as}} = \frac{\alpha_{as}}{\beta_{ms}(B-1)} \quad (2)$$

The result of the inversion is the backscatter ratio and

$$B(\lambda, R) = \frac{\beta_{as} + \beta_{ms}}{\beta_{ms}} = \frac{8\pi.\alpha_{as}}{3S.\alpha_{ms}} \quad (3)$$

The concentration N (in ppm) of the measurement target species in the range between R and R+ΔR can be derived from the following expression, which is known as the DIAL equation (Hering et al., 2003; Thomas, 1995; Fujii and Fukuahi, 2005):

$$N(R) = \frac{10^{12}}{2N_{atm}\Delta\sigma}\frac{\partial}{\partial R}\left(\ln\frac{P_s(\lambda_{off},R)}{P_s(\lambda_{on},R)}\right) - \frac{10^{12}}{2N_{atm}\Delta\sigma}\frac{\partial}{\partial R}\left(\ln\frac{\beta(\lambda_{off},R)}{\beta(\lambda_{on},R)}\right) - \frac{\Delta\alpha_{atm}}{N_{atm}\Delta\sigma}\times 10^{12} \quad (4)$$

Here $\Delta\sigma = \sigma_{abs}(\lambda_{on}) - \sigma_{abs}(\lambda_{off})$ is the differential absorption cross-section of the species of interest, N_{atm}=2.55×10^{19} cm^{-3} is the total number density of molecules in the atmosphere at sea level, and $\Delta\alpha_{atm} = \alpha_{atm}(\lambda_{off}) - \alpha_{atm}(\lambda_{on})$ is the differential extinction coefficient of the atmosphere, describes as

$$\begin{aligned}\Delta\alpha_{atm} = &[\alpha_{ma}(\lambda_{off},R) - \alpha_{ma}(\lambda_{on},R)] + [\alpha_{ms}(\lambda_{off},R) - \alpha_{ms}(\lambda_{on},R)] \\ &+ [\alpha_{as}(\lambda_{off},R) - \alpha_{as}(\lambda_{on},R)]\end{aligned} \quad (5)$$

where $\Delta\alpha_{ms}$, $\Delta\alpha_{ma}$, and $\Delta\alpha_{as}$ are the differential molecular scattering, molecular absorption and aerosol scattering coefficients, respectively.

The two last expressions in the right hand side of Eq. (4) are known as systematic errors. The systematic errors in DIAL measurement can be divided into four categories; (1) differential backscatter errors, (2) differential molecular absorption errors, (3) differential molecular scattering errors, and (4) differential aerosol scattering errors. Errors are caused by the large separation between the on and the off signals and different absorption by gases other than the species of interest and scattering.

In general, each of the terms in Eq. (4) must be known. The main errors of the measurement gas concentration lie with the high aerosol and air molecule concentrations in the troposphere. Most analysis of DIAL measurements ignore the errors due to difference in atmospheric backscattering and aerosol extinction, and Rayleigh scattering at on and off wavelengths. Simplifying conditions can be hold when the on and off wavelengths are close together and differential extinction coefficient of the atmosphere is negligible. Errors are caused by the large wavelength separation between the on and off wavelength of the species of interest. In addition, differential backscatter error is negligible under conditions of spatially

homogeneous backscatter. Hence, if these simplifications cannot be made each of the terms must also be considered.

2.1. Differential molecular absorption

Since the absorption lines of the most atmosphere constituents, such as O_3, O_2, SO_2, H_2O and NO_2 lie in UV/Vis region, the systematic error increases mainly due to different extinction and backscatter properties of the atmosphere at the DIAL probe wavelengths. Among the expected noise from these species in the atmosphere, O_3 is considered as the dominant constituent in the UV region. Fig. 1 shows the absorption spectrum of ozone. The ozone absorption spectrum have a band continuum in the UV (the Hartly band in the range 200-310 nm with a peak at ~255 nm and the Hugins bands in the range 310-350 nm) and, the visible and near infrared (the Chappuis band in the range 400-700 nm with a peak at ~600 nm) spectral region, Molina and Molina, (1986).

In Fig. 2, the dependence of molecular absorption extinction, α_{ma}, on the wavelength is plotted for the ozone density of homogenous concentration of 0.8×10^{12} cm^{-3} near the surface which corresponds to 30 $\mu g/cm^{-3}$ or 30 parts in 10^9 volumes (ppbv). It is evident that maximum molecular absorption extinction at 255 nm is ~1 km^{-1} and reduces rapidly to ~10^{-6} km^{-1} by increasing wavelength neat 360 nm.

Generally, differential absorption errors caused by ozone in UV-DIAL remote sensing can be written as:

$$SE_{ma}(ppm) = 3.92\times10^{-8}\frac{\Delta\alpha_{ma}}{\Delta\sigma} \qquad (6)$$

where $\Delta\alpha_{ma} = \Delta\sigma_{O_3} N_{O_3}$ is differential ozone absorption, N_{O_3} represents the ozone concentration in cm^{-3} and $\Delta\sigma_{O_3}$ is the differential absorption cross-section of ozone.

2.2. Differential molecular scattering

For particles with radius a, smaller than the wavelength of the light, λ, i. e. $\frac{2\pi\pi}{\lambda} << 1$, Rayleigh scattering is observed without absorbing the light. The particle itself is not required to be small, only the ratio a/λ. According to Van de Hulst (1957), McCartney (1976) and

Bodhaine et al. (1999), the classical equation used to calculate the attenuation due to molecular scattering can be written in the following form for nonstandard values of air pressure, temperature:

$$\alpha_{ms} = \frac{24\pi^3}{N_s\lambda^4}\left(\frac{n^2-1}{n^2+2}\right)^2\left(\frac{6+3\rho}{6-7\rho}\right)\left(\frac{T_s/T}{p/p_s}\right)\times 10^5 \quad \text{km}^{-1} \tag{7}$$

where T_s=288.15 (K) and p_s=1 (atm) are temperature and atmospheric pressure of the standard condition, respectively, λ is the wavelength in centimeters, n is the refractive index of air (function of λ), $N_s=2.69\times10^{19}$ cm^{-3} (Loschmidt's number) is the density of molecules in the atmosphere under STP conditions, T(K) is temperature, P(atm) is the atmospheric pressure, and $\rho = I_s^{\perp}/I_s^{\parallel}$ is the depolarization ratio for light scattered at $\pi/2$ as studied by Strutt (1918) and Rayleigh (1920). In this instance the perpendicular and parallel signs refer to the plane of polarization of the incident linearly polarized light beam. According to Zuev (1976), this polarization defect for air molecules is about 0.035 in UV/Vis spectrum and in the case of isotropic scatters such as monatomic gases is zero.

N_S as calculated by Bodhaine et al. (1999) from the Loschmidt constant (defined as the ratio of the Avogadro constant to the molar volume of an ideal gas) yields as the molecular number density for standard air conditions.

For 23 ℃ at sea level (1 atm pressure) Eq. (7) reduces to:

$$\alpha_{ms} = (2.973\times10^{-12})\frac{(n^2-1)^2}{(n^2+2)^2}\frac{1}{\lambda^4} \quad \text{km}^{-1} \tag{8}$$

where n is a function of λ. For arbitrary values of temperature T and pressure p, the refractive index of air is given by Penndorf (1957):

$$n = 1+(n_s-1)\frac{T_s/T}{P/P_s} \tag{9}$$

where n_s is the refractive index of standard air at STP conditions and is given by Edlén (1966):

$$(n_s-1) = 8342.13\times10^{-8} + \frac{2{,}406{,}030}{130\times10^8 - \lambda^{-2}} + \frac{15{,}997}{38.9\times10^8 - \lambda^{-2}} \tag{10}$$

with λ measured in centimeter. A more accurate formulation that considers water vapor and CO_2 content can be found by Tomasi et al. (2005). These two variables have negligible effects in comparison with the influences caused by temperature and the atmospheric pressure (Penndorf, 1957; Edlén, 1966), and for the sake of simplicity, they are not taken into account in this study.

In Fig. 3, the dependence of molecular scattering extinction, α_{ms}, on the wavelength is plotted for T=300 K, P=1 atm. It can be seen α_{ms}, slowly reduces from ~0.8 km^{-1} to 0.04 km^{-1} by increasing wavelength between 200-400 nm.

Generally, differential molecular scattering errors can be written as:

$$SE_{ms}(\text{ppm}) = 3.92\times10^{-8}\,\frac{\Delta\alpha_{ms}}{\Delta\sigma} \tag{11}$$

2.3. Differential aerosol scattering

In the presence of particles with a size comparable to the incident wavelength, the Mie scattering becomes predominant. Its efficiency is generally much bigger than the Rayleigh's one. The strong Mie-scatter behavior of the absorption aerosol allows an easy lidar observation. Mie scattering takes place at particles of sizes of order of the light wavelength. For large particles forward scattering is more probable than backward-direction scattering. The scattering losses can be much larger than the Rayleigh scattering losses if enough particles are present.

The scattering intensity and angular distribution is a complicated function of the particle sizes distributions and complex refractive indices. Aerosol scattering can be explained by the Mie theory (Van de Hulst, (1957), which studies the interaction between an electromagnetic wave and a spherical particle (absorbent or non-absorbent) of given size and refractive index. In order to predict the aerosol extinction by this theory it is necessary to have an approximate knowledge of the distribution of aerosol particles across the propagation path of the optical radiation, which is impossible in most of the practical cases. A feasible way of calculating the aerosol scattering coefficient is expressing it in function of the visibility or visual range V, that is defined as the distance from which an observer can discern an object against the

horizon sky (Faxvog, 1978; Middleton, 1952). The aerosol scattering coefficient based on empirical fit to short wavelength transition data by considering uniform characteristics of particle size and species is given by Kruse (1963), Patterson and Gillespie (1989):

$$\alpha_{as} = \left[\frac{C}{V} - \alpha_{ms}(550\,\text{nm})\right]\left[\frac{\lambda}{550\,\text{nm}}\right]^{-0.585V^{1/3}} \quad \text{km}^{-1} \tag{12}$$

where α_{ms} (550 nm)=0.01045 km^{-1}, C=3.912, λ has to be expressed in nm and V in km is the horizontal visual range. Because the visibility depends on the total atmospheric extinction coefficient, the molecular attenuation (scattering and absorption) at 550 nm has been subtracted from the total atmospheric attenuation coefficient to determine the particle extinction.

In Eq. (12) the effect of aerosol absorption has been included. Most aerosol particles slightly absorb optical radiation. However, extinction by aerosol particles is exclusively due to scattering.

In Fig. 4, the aerosol scattering extinction is plotted as a function of wavelength for three distinct visibility conditions, V=0. 5 km, V=1 km and 1.5 km. In this figure, the dashed and dotted line corresponds to a V=1.5 km, the dotted line to a V=1 km and the solid line to a V=1.5 km. It is evident, particle attenuation increases with decreasing visibility which reduced visibilities are associated with larger particles. The molecular scattering extinction decreases rapidly with increase in the wavelength while aerosol scattering decreases smoothly.

A plot of attenuation due to ozone absorption, molecular scattering and sum of them as a function of wavelength is shown in Fig. 5. The molecular scattering coefficient is given by dashed and dotted line, the ozone absorption coefficient by dashed line and sum of then by solid line. It is evident, at the higher altitudes (>30 km) that the aerosol concentration is low, the molecular scattering is dominant in the range of ~310-400 nm. Therefore, in the stratosphere that the aerosol density is much lower, fluorescence lidar has been found useful to measure the trace atmospheric constituents from the ground and space.

In Fig. 6 the aerosol scattering attenuation as a function of wavelength for different visibility conditions (0.5 km, 1 km, 1.5 km), the molecular scattering attenuation and dotted line and the ozone absorption attenuation is shown. In this figure, the crossed line corresponds to a V=1.5 km, the circled line to a V=1 km, the pointed line to a V=1.5 km, the dashed and dotted line to the molecular scattering and dotted line to the ozone absorption attenuation. Obviously, as the visibility gets worse, the attenuation decreases. For all the visibility conditions studied, the attenuation due to aerosol is dominant in lower atmosphere. Since aerosol concentration is quite large at low altitudes and decreases very rapidly with altitude, thereby giving very large backscattered signal from lower atmosphere scattering by aerosols (Mie scattering) is dominant, especially for large value of visibility. Finally, the total attenuation for several values of visibility is listed from 200-400 nm.

Conclusion

In this work, we attempt to determine atmospheric attenuation coefficients that limit both the sensitivity and accuracy of lidar measurements. In the lower atmosphere aerosol scattering (Mie scattering) is dominant, especially for large value of visibility, whereas at higher altitudes (> 30 km) scattering by air molecules is only important especially for wavelength larger 310 nm. In the near surface, the aerosol scattering can be important and indeed limit the penetration depth of a probing laser beam.

Data present here is useful to chose laser wavelength such that it does not have absorption band of any molecule/specie; except for certain applications where absorption mechanism is important. These results are even true for differential absorption lidar (DIAL) technique where both absorption and scattering are present. It is found that in remote sensing by DIAL, the systematic error due to aerosol scattering is negligible even separation of two wavelengths is sufficient. Errors can arise when the wavelengths are significantly separated and there is range dependence (inhomogeneity) in the aerosol scattering distribution.

References

Bodhaine, B. A. Wood, N. B. Dutton, E. G. Slusser, J. R. (1999). On Rayleigh optical depth calculations. *J. Atmos. Oceanic Techno., 16,* 1854–1861.

Beniston, M. Wolf, J. P. Beniston-Rebertz, M. Kolsch, H. J. Rairoux, P. Woste, L.(1990) Use of lidar measurements and numerical model in air pollution research. *J. Geophys. Res. 95,* 9879-9894.

Browell, E. V. Higdon, N. S. & Ismail, S. (1991). Raman shifting of KrF laser radiation for tropospheric ozone measurements. *Appl. Opt., 30,* 2628-2633.

Camagani P. & Sandroni, S. (1984). Optical remote sensing of the air pollution. B V, (pp 123-150). Elsevier Science Publisher.

Dell'Aglio, M. Kholodnykh, A. Lassandro, R. De Pascale, O. (2002). Development of a Ti:Sapphire DIAL system for pollutant monitoring and metrological applications. *Optics and Laser Engineering, 37,* 233-144.

Demtröder, W. (2003). Laser Spectroscopy: Basic concepts and Instrumentation, 3rd Edition, Springer.

Derava, P. Raj, P. E. Padithurai, G. Dani, K. K. Sonbawne, S. M. (2004) Excimer-Raman DIAL probing of atmospheric ozone over an urban station: First result, In: Proceeding. of 22nd International Laser Radar Conference, (Italy, Matara).

Edlén, B. (1966). The refractive index of air. *Metrologia 2,* 71–80.

Edner, H. Fredriksoon, K. Sunesson, A. Svanberg, S. Uneus, L. Wendt, W. (1987). Mobile remote sensing system for atmospheric monitoring. *Appl. Opt. 26,* 4330-4338.

Edner, H. Paris, G. W. Sunnesson J. A. Svanberg, S. (1989). Atmospheric atomic mercury monitoring using differential absorption lidar techniques. *Appl. Opt. 28,* 921-930.

Egeback, A. Fredriksson, K. & Hertz, H. (1984). DIAL techniques for the control of sulfur dioxide emission. *Appl. Opt. 23,* 722-729.

Faxvog, F.R. (1978). Carbon aerosol visibility vs particle size distribution. *Appl. Opt. 17,* 2612–2616.

Fugii, T. Fukuchi, T. Goto, N. Nemoto, K. Takeuchi, N. (2001). Dual differential absorption lidar for the measurement of atmospheric SO_2 of the order of parts in 10^9. *Appl. Opt. 40,* 949-956.

Fujii, T. & Fukuahi, T. (2005). Laser Remote Sensing. Taylor & Francis Group.

Hering, P. Lay, J. P. & Stry, S. (Eds.), (2003). Laser in environmental and life sciences: Modern analytical method. Springer, Heidelberg-Berlin.

Holton, J. R. Pyle, J. & Currie J. A. (Eds.), (2002). Encyclopedia of atmospheric sciences. Academic Press.

Kobayashi, T. Imaki, M. Takegoshi, Y. Sugimoto, N. (2004). UV high-spectral-resolution lidar for absolute measurement of aerosol extinction coefficient and lidar-ratio. In: *Proceeding. of 22nd International Laser Radar Conference,* (Italy, Matara).

Kruse, P.W. McGlauchin, L.D. McQuistan, R.B. (1963). Elements of Infrared Technology. New York: Wiley.

Mandelis, A. & Hess, P. (Eds.), (1997). Progress in photochemical and photoacoustic science and technology. Vol. III, *Life and Earth Science*, SPIE, Optical Engineering Press, Washington.

McCartney, E. J. (1976). Optics of the Atmosphere, Scattering by Molecules and Particles (pp. 176–215) New York: Wiley.

Meyers, R. A. (Ed.), (2000). Encyclopedia of analytical chemistry. Chichester:Wiley.

Middleton, W. E. K. (1952). Vision Through the Atmosphere. University of Toronto Press, Toronto.

Milton, M. et al., (1992). Measurements of toluene and other aromatic hydrocarbons by a differential-absorption LIDAR in the near ultraviolet. *Appl. Phys. B, 55,* PP. 41-41.

Molina, L.T. & Molina, M.J. (1986). Absolute absorption cross-sections of ozone in the 185- to 350-nm wavelength range. *Journal of Geophysical Research 91 (D13), 14,* 501–08.

Moosmüller, et al., (1992). Ozone measurements with the U.S. EPA UV-DIAL: Preliminary results. *In: Abstracts, Sixteenth International Laser Radar Conf., MIT, Cambridge, Ma., July 20-24, NASA Conf. Pub. 3158,* 95-99.

Moosmüller, et al., (1994). An airborne UV-DIAL system for ozone measurements: Field use and verification. In: *Optical Sensing for Environmental Monitoring*, SP-89, Air & Waste Management Assoc., 413-422.

Patterson, E.M. & Gillespie, J.B. (1989). Simplified ultraviolet and visible wavelength atmospheric propagation model. *Appl. Opt. 28*, 425–429.

Penndorf, R. (1957). Tables of the refractive index for standard air and the Rayleigh scattering coefficient for the spectra region between 0.2 and 20 μmand their application to atmospheric optics. *J. Opt. Soc. Am. 47*, 176–182.

Rayleigh, L (1920). A re-examination of the light scattered by gases in respect of polarization. I. Experiments on the common gases. *Proc Roy Soc London, 97*, 435–450.

Rothe, K. W. Brinkmann U. & Walther, H. (1992). *Appl. Phys. B, 54*, 89.

Sigrist, M. W. (Ed.), (1994). Air monitoring by spectroscopic techniques. *Chemical Analysis Series*, 127, New York:Wiley.

Strutt R. J. (1918). The light scattered by gases: its polarization and intensity. *Proc. Roy. Soc. London, 95*,155–176.

Thomas, L. (1995). Lidar methods and applications, in Spectroscopy in Environmental Science, Clark, R.J.H. & Hester, R.E. (Eds.), Wiley, Chichester.

Tomasi C, Vitale V, Petkov B, Lupi A, & Cacciari A (2005). Improved algorithm for calculations of Rayleigh-scattering depth in standard atmosphere. *Appl. Opt. 44*, 3320-3341.

Uchino, O. (2006). On some lidar developments for atmospheric research. In: *Proceeding. of 23rd International Laser Radar Conference*, (Japan, Nara).

Van de Hulst, H. C. (1957). Light Scattering by Small Particles. (pp. 63–84) New York: Wiley.

Veselovskii, I. & Barchunov, B. (1999). Excimer-laser-based lidar for troposphere ozone monitoring. *Appl. Phys. B, 68*, 1131-1137.

Weitkamp, C., (Ed.), (2005). Lidar: Range-Resolved Optical Remote Sensing of the Atmosphere. New York: John Wiley & Sons.

Wolf, J. P. Dounard, M. Fritzsche, K. Rairoux, P. Ulbricht, G. Weidaurer, D. Woste, L. (1993). 3D-monitoring of air pollution using all solid state lidar system. *Proc. SPIE, 2112*, 147-158.

Zanzottera, E. (1990). Differential absorption lidar technique in the detection of trace pollutants and physical parameters of the atmosphere. *Crit. Rev. Anal. Chem., 21*, .

Zuev, Y. E. (1976). Laser light transmission through the atmosphere. *Laser monitoring of the atmosphere*, Hinckly, E. D. (ed.), Springer-Verlag.

Figure captions

Fig.1 The absorption cross-section of ozone as a function of wavelength [29].

Fig.2 The ozone absorption extinction as a function of wavelength.

Fig.3. Molecular scattering for 23 ℃ at sea level as a function of wavelength.

4. Aerosol scattering as a function of wavelength for V=0.5 km (dashed and dotted line), V=1 km (dotted line), and V=1.5 km (solid line).

Fig. 5. Attenuation due to ozone absorption (dashed line), molecular scattering (dashed and dotted line) and sum of them (solid line) as a function of wavelength.

Fig. 6. Aerosol scattering attenuation as a function of wavelength for V=0.5 km (pointed line), V=1 km (circled line), and V=1.5 km (crossed line); the molecular scattering attenuation is given by dashed and dotted line and the ozone absorption attenuation by dotted line.

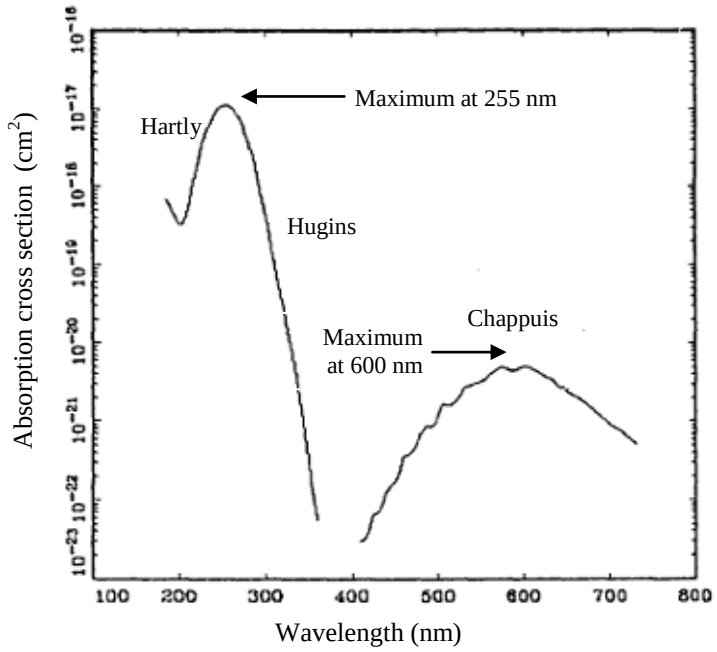

Fig.1 The absorption cross-section of ozone as a function of wavelength [29].

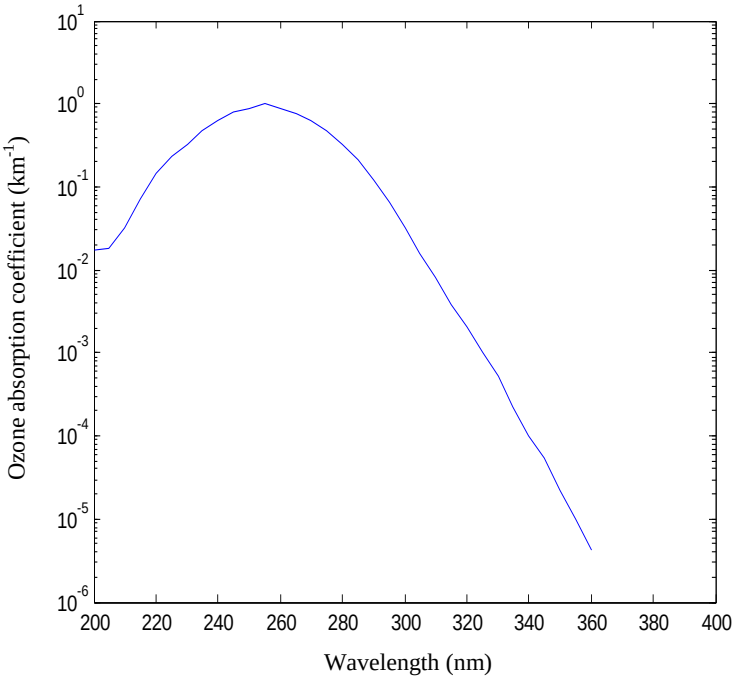

Fig.2 The ozone absorption extinction as a function of wavelength.

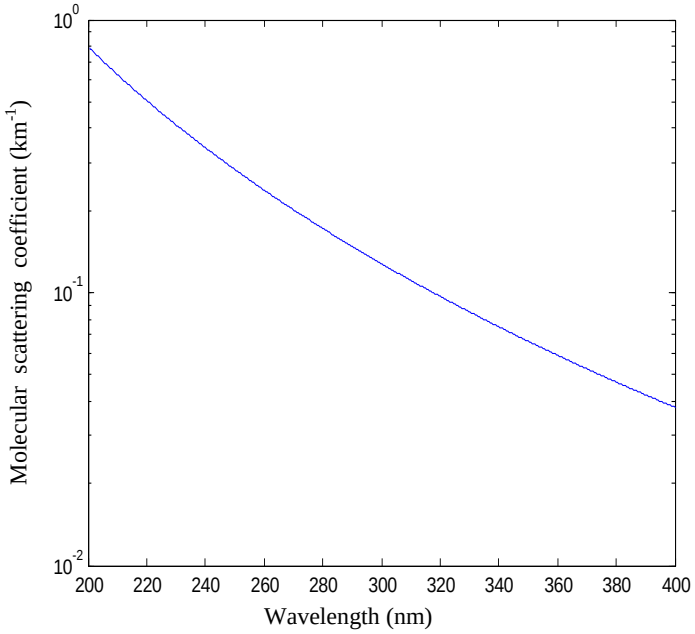

Fig.3. Molecular scattering for 23 ℃ at sea level as a function of wavelength.

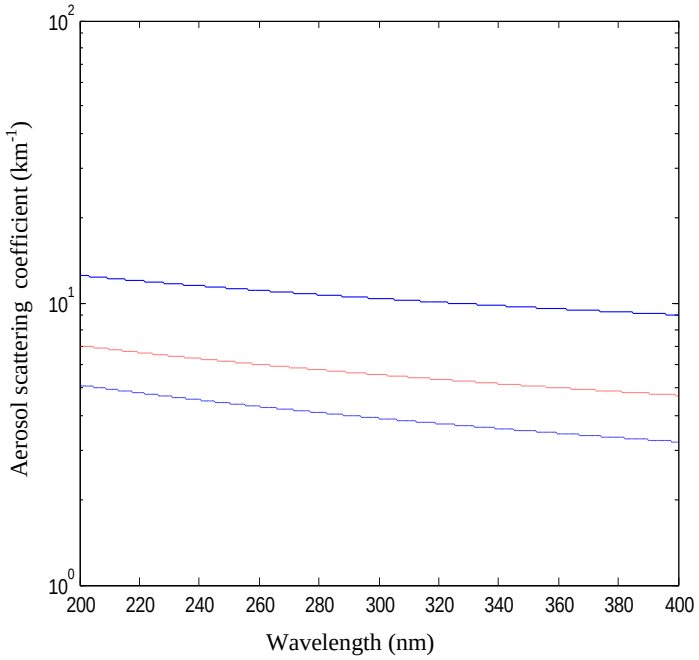

Fig. 4. Aerosol scattering as a function of wavelength for V=0.5 km (dashed and dotted line), V=1 km (dotted line), and V=1.5 km (solid line).

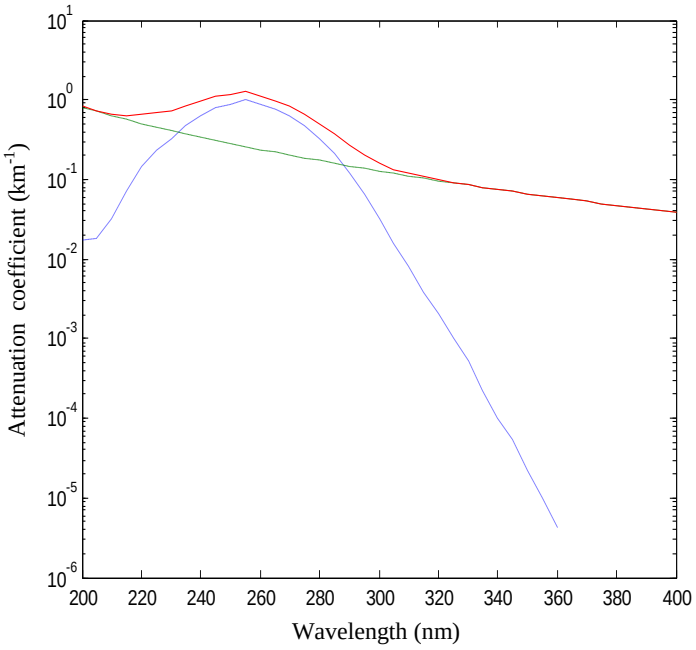

Fig. 5. Attenuation due to ozone absorption (dashed line), molecular scattering (dashed and dotted line) and sum of them (solid line) for 23 ℃ at sea level as a function of wavelength.

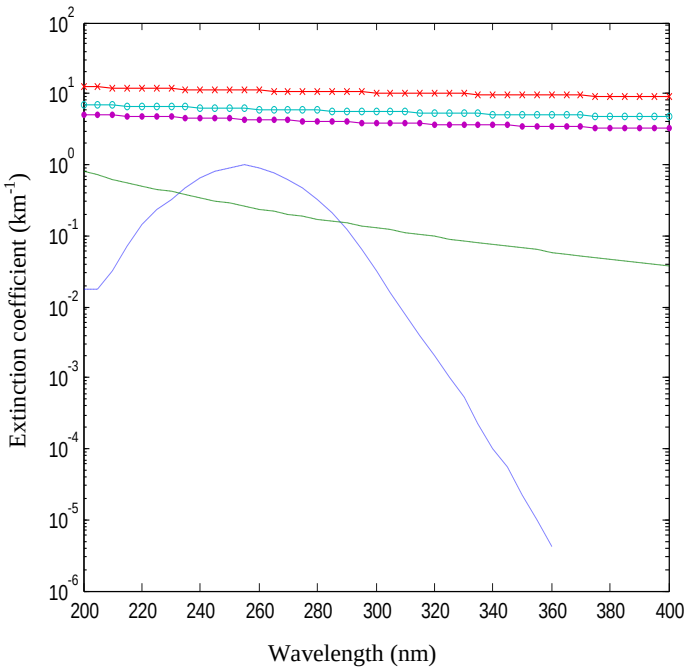

Fig. 6. Aerosol scattering attenuation as a function of wavelength for V=0.5 km (pointed line), V=1 km (circled line), and V=1.5 km (crossed line); the molecular scattering attenuation is given by dashed and dotted line and the ozone absorption attenuation by dotted line.

Table 1: Total attenuation due to aerosol attenuation, molecular scattering and molecular absorption for 23 ℃ at sea level for different visibility conditions and wavelengths.

Wavelength (nm)	Total attenuation (km^{-1})					
	V=0.5 km	V=1 km	V=1.5 km	V=5 km	V=10 km	V=15 km
200	13.3156	7.8686	5.9318	2.9413	2.1802	1.8951
205	13.0826	7.6770	5.7574	2.7990	2.0480	1.7669
210	12.8816	7.5162	5.6133	2.6861	1.9449	1.6678
215	12.7222	7.3958	5.5093	2.6124	1.8808	1.6077
220	12.6082	7.3199	5.4492	2.5818	1.8596	1.5903
225	12.5219	7.2706	5.4153	2.5766	1.8637	1.5981
230	12.4458	7.2306	5.3903	2.5797	1.8757	1.6139
235	12.4508	7.2707	5.4451	2.6618	1.9665	1.7084
240	12.4640	7.3181	5.5068	2.7501	2.0634	1.8088
245	12.4844	7.3720	5.5746	2.8438	2.1654	1.9143
250	12.4314	7.3516	5.5678	2.8623	2.1921	1.9444
255	12.4244	7.3765	5.6059	2.9251	2.2628	2.0185
260	12.1828	7.1660	5.4084	2.7517	2.0972	1.8562
265	11.9462	6.9598	5.2148	2.5817	1.9348	1.6970
270	11.7062	6.7495	5.0169	2.4068	1.7673	1.5327
275	11.4464	6.5188	4.7982	2.2106	1.5784	1.3469
280	11.1865	6.2874	4.5786	2.0130	1.3879	1.1594
285	10.9703	6.0990	4.4018	1.8576	1.2395	1.0139
290	10.7855	5.9414	4.2555	1.7324	1.1210	0.8983
295	10.6358	5.8185	4.1436	1.6410	1.0364	0.8165
300	10.5131	5.7219	4.0579	1.5754	0.9773	0.7602
305	10.4092	5.6437	3.9903	1.5275	0.9357	0.7213
310	10.3159	5.5755	3.9325	1.4890	0.9034	0.6917
315	10.2290	5.5132	3.8804	1.4558	0.8763	0.6671
320	10.1468	5.4551	3.8323	1.4262	0.8527	0.6461
325	10.0674	5.3995	3.7865	1.3985	0.8309	0.6267
330	9.9908	5.3461	3.7428	1.3725	0.8106	0.6089
335	9.9163	5.2945	3.7006	1.3478	0.7914	0.5921
340	9.8439	5.2446	3.6599	1.3242	0.7733	0.5763
345	9.7734	5.1961	3.6205	1.3015	0.7560	0.5613
350	9.7046	5.1489	3.5822	1.2798	0.7395	0.5471
355	9.6375	5.1031	3.5451	1.2588	0.7238	0.5335
360	9.5719	5.0584	3.5091	1.2386	0.7086	0.5205
365	9.5079	5.0149	3.4741	1.2191	0.6941	0.5081
370	9.4453	4.9725	3.4400	1.2003	0.6802	0.4962
375	9.3840	4.9312	3.4068	1.1821	0.6668	0.4848
380	9.3241	4.8908	3.3745	1.1646	0.6539	0.4739
385	9.2655	4.8514	3.3430	1.1475	0.6415	0.4634
390	9.2081	4.8129	3.3122	1.1311	0.6295	0.4534
395	9.1518	4.7753	3.2823	1.1151	0.6180	0.4437
400	9.0967	4.7386	3.2531	1.0996	0.6069	0.4344